# New Dirac Fermions in Periodically Modulated Bilayer Graphene

Liang Z. Tan, Cheol-Hwan Park, and Steven G. Louie*

Department of Physics, University of California, Berkeley, California 94720, United States and Materials Sciences Division, Lawrence Berkeley National Laboratory, Berkeley, California 94720, United States

ABSTRACT: We investigate the effect of periodic potentials on the electronic structure of bilayer graphene and show that there is a critical value of the external potential below which new Dirac fermions are generated in the low-energy band structure, and above which a band gap is opened in the system. Our results, obtained from a self-consistent tight-binding calculation, can be simply explained by a two-band continuum model as a consequence of the pseudospin physics in graphene. The findings are robust against changes in the form of the potential, as well as bias voltages between the layers.

KEYWORDS: Bilayer graphene, superlattice, periodic modulation, Dirac fermions, zero-energy modes, quantum phase transition
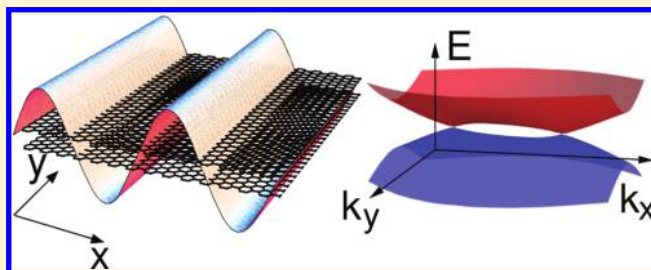
Monolayer and bilayer graphene are atomically thin carbon crystals that have generated intensive research effort in recent years. Monolayer graphene has an unusual Dirac cone band structure at low energies,[1−3] while bilayer graphene is a parabolic band material with zero band gap.[4,5] Both monolayer and bilayer graphene have tunable electronic properties that may be controlled by different techniques, which among others include strain,[6,7] patterning,[8−10] and the application of external electric[11−19] and magnetic fields.[20−26] Because of this flexibility and tunability in their electronic structure, both materials are of great promise as platforms for nanoscale carbon-based electronics.[27]

One method of modifying the electronic structure of monolayer and bilayer graphene is by constructing a superlattice, that is, applying external perturbations which result in a structure with periodicity much larger than that of the underlying honeycomb lattice of graphene. Such monolayer graphene superlattices have been constructed for graphene on ruthenium[28−30] and iridium[31−33] surfaces, for example. Other possible techniques for creating superlattices that may also be applicable to bilayer graphene include lithography,[34] as well as the use of periodically patterned gates. The effect of a periodic external potential on the electronic structure of monolayer graphene has been studied in some detail in refs 11−14, where it has been shown that a sufficiently strong periodically modulated potential can drastically modify the group velocity of the carriers and generate new zero-energy modes at different k-points (Dirac points) in the Brillouin zone.

Similarly, it has been shown[14,15] that the effect of a series of δ-function potentials on bilayer graphene is to either open an energy gap or to generate new zero energy modes in the electronic structure, depending on the strength and periodicity of the δ-functions. In this paper, we demonstrate that this behavior is robust against charge screening effects, as well as being present for a wide range of shapes of the external potential. We show that unlike the case of monolayer graphene,[11−13] a strong external

potential is not needed for the generation of new Dirac points. In fact, these new zero-energy modes can be generated at arbitrarily weak periodic external potentials. The transition from this new semimetallic state with Dirac points to the previously found semiconducting state[14] occurs at a critical value of the external potential. Finally, further increase of the external potential closes the band gap and a semimetallic band-structure is restored, albeit with Dirac points in different locations in reciprocal space than before.

We note that similar physics arises in twisted graphene bilayers[35−41] where a new pair of Dirac points is generated at each valley. Unlike the case considered in this paper, the Dirac points in the twisted graphene bilayers are topologically protected against breaking of the interlayer symmetry, as a result of the low energy Hamiltonian belonging to a different universality class than the one considered in this paper.[41]

We begin our analysis of bilayer graphene superlattices (with the two layers in the Bernal stacking) with a two-band continuum model for the lowest energy electron and hole states in a bilayer system, given by the Hamiltonian

$$H = -\frac{1}{2m}\begin{pmatrix} 0 & (p_x - ip_y)^2 \\ (p_x + ip_y)^2 & 0 \end{pmatrix} + V(x)\begin{pmatrix} 1 & 0 \\ 0 & 1 \end{pmatrix}$$

(1)

where $\vec{p} = -i\hbar\vec{\nabla}$, $m = \gamma_1/(2v_F^2)$ is the effective mass in bilayer graphene, γ_1 is the interlayer tunneling amplitude and v_F is the Fermi velocity of graphene.[16] The one-dimensional external periodic potential $V(x)$ is assumed to average to zero and has large periodicity compared to the interatomic distance. The potential on both graphene layers is taken to be the same at a
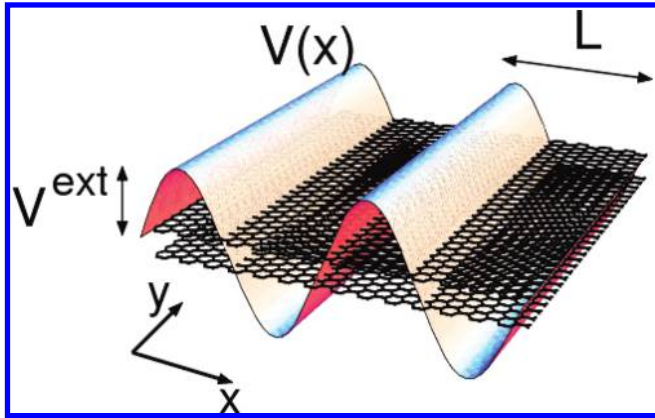
Figure 1. Schematic of bilayer graphene in an external sinusoidal potential $V(x)$, with period L and amplitude V^{ext}. The external potential is constant along the y-direction. L is much larger than the lattice constant of bilayer graphene, and $V(x)$ is taken to be the same on both layers.

given point (x,y). (Later, we discuss the case where this symmetry is broken.) Analyzing the effect of $V(x)$ on the low energy carriers in this manner is justified if its period is much larger than the lattice constant $a = 0.246$ nm in graphene (Figure 1). Inter-valley scattering is then negligible and eq 1 describes a single, independent valley. In this initial analysis, for simplicity the external periodic potential is taken to be of the form $V(x) = V^{\text{ext}}$ $\sin(2\pi x/L)$. Use of a two-band model in the form of eq 1 neglects the effect of trigonal warping. As will be seen from our tight-binding calculations below, such effects do not change the nature of our results.

We have performed a numerical diagonalization of eq 1, using as a basis the eigenstates of pristine bilayer graphene (i.e., with $V(x) = 0$ in eq 1)

$$|\psi^{(0)}(\vec{k})\rangle = \frac{1}{\sqrt{2}}\begin{pmatrix} 1 \\ \pm e^{2i\theta_k} \end{pmatrix} e^{i\vec{k}\cdot\vec{r}} \qquad (2)$$

where $\vec{k}$ and $\vec{r}$ are two-dimensional vectors and $\tan\theta_{\vec{k}} = k_y/k_x$ and the $+$ and $-$ signs refer to the conduction and valence bands, respectively. At low values of V^{ext}, a pair of zero energy modes are generated along the $k_y = 0$ line (Figure 2) symmetrically at different values of k_x depending on the strength of V^{ext}. At these values of V^{ext}, these are the only zero energy modes, as seen in Figure 2a. The band structure close to these zero energy modes is Dirac-cone like, with a k-space anisotropy that is dependent on the value of V^{ext}. As V^{ext} is increased from zero, this pair of zero energy modes are initially generated near the $\vec{k} = 0$ point of the superlattice Brillouin zone (i.e., the K or K' point of the original Brillouin zone of bilayer graphene), and they move in opposite directions away from the $\vec{k} = 0$ point as V^{ext} is increased (Figure 2b−d) but always keeping $k_y = 0$. At a certain value of V^{ext}, both zero energy modes reach the edge of the supercell Brillouin zone. Further increase in V^{ext} opens a direct band gap at $(k_x = \pm \pi/L, k_y = 0)$, where L is the superlattice period (Figure 2e). In general, the critical value $V^{\text{ext}} = V^*$ at which the gap opens depends on L in the following manner

$$V^* = CE_L \qquad (3)$$

where $E_L = \hbar^2/(2mL^2)$ and C is a numerical constant determined by the shape of the external potential, as we show later (see eq 11).
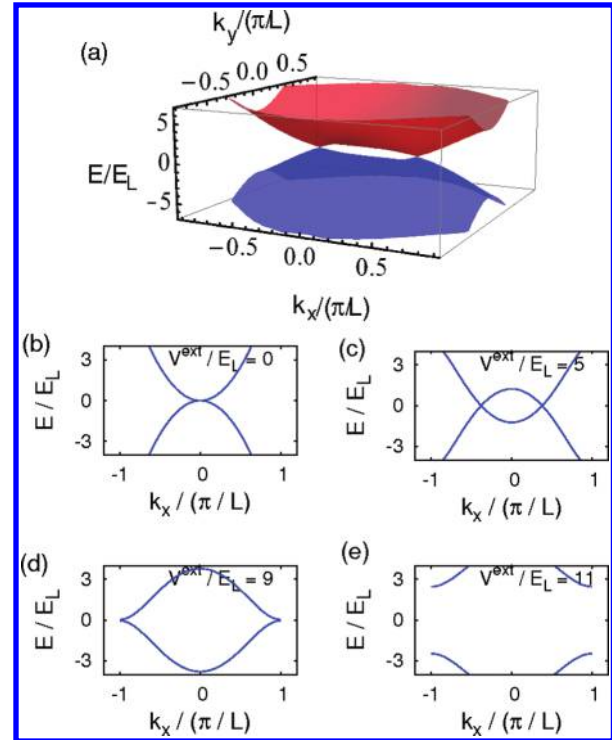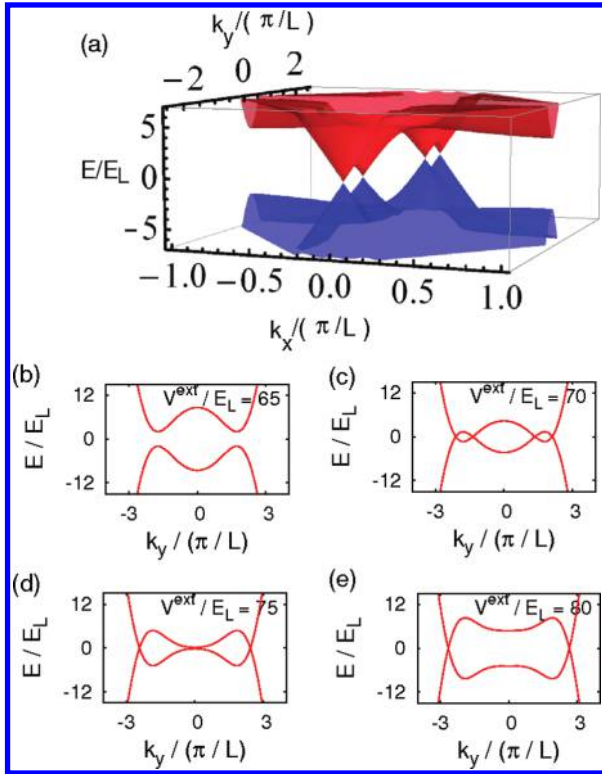

Figure 2. The band structure of bilayer graphene superlattice for the case of $V(x) = V^{\text{ext}}\sin(2\pi x/L)$ with $V^{\text{ext}} < V^*$ (see text) calculated within the two-band continuum model. A pair of Dirac points is shown in (a), where the lowest valence and conduction bands are plotted in the first Brillouin zone of the superlattice and the magnitude of the external potential is $V^{\text{ext}} = 5E_L$ where $E_L = \hbar^2/(2mL^2)$. (b−e) Panels show cuts of the band structure along the $k_y = 0$ plane for various magnitudes of the external potential V^{ext}. The band structure of pristine bilayer graphene is shown in (b).

The band gap opened at $V^{\text{ext}} = V^*$ continues to increase with increasing V until it reaches a maximum value. Thereafter, the band gap decreases with increasing V and it eventually vanishes. The closing of the band gap corresponds to generation of new Dirac points along the $k_x = 0$ line, as illustrated by Figure 3c−e. At the higher value of V^{ext}, the system remains in a semi-metallic state as V^{ext} increases because some of the new Dirac points persist with increasing V^{ext} (Figure 3e).

The generation of new Dirac points in the limit of low V^{ext} (Figure 2) can be understood as a consequence of the specific pseudospin structure of the eigenstates of bilayer graphene. Within second order perturbation theory (the first order term vanishes), the effect of the superlattice potential is to cause a shift of the conduction band by an amount

$$E_c^{(2)}(\vec{k}) = \sum_{\substack{i=c,v \\ \vec{G}}} \frac{|\Delta V_{\vec{k},\,\vec{k}+\vec{G}}^{c,i}|^2}{E_c^{(0)}(\vec{k}) - E_i^{(0)}(\vec{k} + \vec{G})} \qquad (4)$$

where $E_i^{(0)}(\vec{k})$ are the band energies of the conduction or valence band of pristine bilayer graphene, **G** are the superlattice reciprocal lattice vectors, and $V_{\vec{k},\vec{k}+\vec{G}}^{c,i}$ is a matrix element of $V(x)$ using the unperturbed states $|\psi^{(0)}(\vec{k})\rangle$ and $|\psi^{(0)}(\vec{k} + \vec{G})\rangle$ given by eq 2. Consider $E_c^{(2)}(\vec{k})$ for a point on the $k_y = 0$ line. Because of the spinor structure of the electronic wavefucntions (the pseudospin

Figure 3. The band structure of bilayer graphene superlattice for selected $V^{ext} > V^*$ calculated for $V(x) = V^{ext} \sin(2\pi x/L)$ within the two-band continuum model. Two pairs of new Dirac points are shown in (a), where lowest valence and conduction bands are plotted in the first Brillouin zone of the superlattice and the magnitude of the external potential is $V^{ext} = 70E_L$ where $E_L = \hbar^2/(2mL^2)$. (b–e) Panels show cuts of the band structure along the $k_x = 0$ plane, for various magnitudes of V^{ext}.

factor in eq 2), the matrix element in eq 4 is nonzero only between those states from the same band (i.e., $V_{\vec{k},\vec{k}+\vec{G}}^{c,v} = 0$, but $V_{\vec{k},\vec{k}+\vec{G}}^{c,c} \neq 0$). From eq 4, it follows that the energy of the conduction band is reduced and the energy of the valence band increased, leading to their overlap and the formation of Dirac points. When $V^{ext} > V^*$, the lowest conduction subband and the highest valence subband of the superlattice are shifted to the extent that the former lies below the latter in energy and a band gap is opened as a result.

While the two-band continuum Hamiltonian (eq 1) provides a simple explanation for the generation of new Dirac points at low value of V^{ext} and the opening of the band gap at $V^{ext} = V^*$ and above, it is not sufficient for more quantitative predictions due to the neglect of the effects of the higher bands and of electronic screening. To address this issue, we have performed a tight binding calculation, which takes into account the effect of the four bands arising from the p_z orbitals of the four carbon atoms in the Bernal bilayer unit cell. We have included the charge transfer and screening effects via a self-consistent Hartree potential. The tight-binding Hamiltonian is of the form

$$ H = \sum_{<i,j>} t_{ij}(c_i^+ c_j + c_j^+ c_i) + \sum_i (V_i^{ext} + V_i^{Hartree}) c_i^+ c_i \quad (5) $$

where c_i, c_i^+ are the electron annihilation and creation operators for site i, t_{ij} the hopping parameter between nearest neighboring sites i and j, V_i^{ext} and $V_i^{Hartree}$ the external and Hartree potentials, respectively. For the intralayer nearest-neighbor hopping amplitude, the value $\gamma_0 = t_{AB} = 2.6$ eV is used, while the interlayer
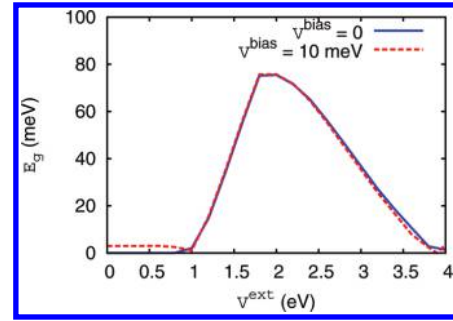
Figure 4. The band gap of bilayer graphene superlattice as a function of the magnitude of the external potential $V(x) = V^{ext} \sin(2\pi x/L)$ obtained from self-consistent tight binding calculations for $L = 15$ nm. The results for systems with and without a bias potential between the two graphene layers are plotted in red dashed and blue solid lines, respectively.

tunneling amplitudes $\gamma_1 = t_{\tilde{A}B}$ and $\gamma_3 = t_{A\tilde{B}}$ are set at 0.34 and 0.3 eV respectively. Here A and B ($\tilde{A}$ and $\tilde{B}$) denote the two atoms in the unit cell on the lower (upper) layer. See ref 19 for a definition of the notation and a justification of these numerical values. A sinusoidal form $V_i^{ext} = V^{ext} \sin(2\pi x_i/L)$ is used for the external potential, where x_i denotes the x coordinate of the ith atomic site. For results discussed below, we have used a value of $L = 15$ nm. The Hartree potential is given by

$$ V_i^{Hartree} = \sum_{\alpha l} \int_{A_\alpha} d^2 r \frac{e n_{\alpha l}}{|\vec{r} - \vec{r}_i|} \quad (6) $$

where the index α refers to a specific unit cell of a single graphene layer, $l = 1$ or 2 is the layer index, A_α is the area of the unit cell (which is the same for all α), and $n_{\alpha l}$ is the net charge density (induced by the superlattice potential) in this particular unit cell that is approximated to be uniform within the cell. The excess electron density depends on the wave functions as

$$ n_{\alpha l} A_\alpha = 2 \sum_{i \in A_{\alpha l}} \sum_{j \in occ.} \int_{BZ} \frac{d^2 k}{(2\pi)^2} |\psi_{i,j}(\mathbf{k})|^2 - N_{\alpha l} \quad (7) $$

Here, $\psi_{i,j}(\mathbf{k})$ is the amplitude of an eigenstate of eq 5 at site i, of the energy band j, and with wavevector $\mathbf{k}$. The sum over i in eq 7 runs over both sites in the single-layer unit cell $A_{\alpha l}$ and the sum over j runs over all occupied energy bands. $N_{\alpha l}$ is the number of π electrons in a unit cell of a single layer, that is, $N_{\alpha l} = 2$. The factor of 2 in eq 7 arises from spin degeneracy. We solve eqs 5–7 self-consistently to find the tight-binding energy bands in the presence of the superlattice potential. The energy eigenvalues are converged to within 1 meV with respect to the k-grid sampling for the two-dimensional momentum space integration.

The results of the self-consistent tight-binding calculation show that the basic picture presented above for the two-band continuum Hamiltonian remains unchanged, except for some quantitative changes. We plot the band gap as a function of V^{ext} in Figure 4 for a superlattice period of $L = 15$ nm. There is no band gap for low V^{ext}, up to a value of $V^{ext*} \approx 0.8$ eV. (With $L = 15$ nm, the value for E_L is 5 meV.) An examination of the low energy band structure (not shown in Figure 4) shows that for this range of V^{ext}, a pair of new Dirac points is generated for each K and K' valley, consistent with the calculations based on the two-band continuum Hamiltonian. Similarly, the opening of a band gap for intermediate V^{ext} (0.8 eV ≤ V^{ext} ≤ 4 eV in Figure 4) and its

subsequent closure at higher V^{ext} are features in agreement with the two-band continuum Hamiltonian.

We have found that the effect of Hartree-level screening can be well described by a dielectric constant. For L = 15 nm, the in-plane dielectric constant (describing screening along the graphene layers rather than between)

$$\varepsilon = \frac{V^{ext}}{V^{ext} + V^{Hartree}} \approx 11 \qquad (8)$$

is approximately constant for the range of V^{ext} shown in Figure 4. Screening is the main reason for the increase in the value of V^{ext*} from the two-band model value of 45 meV to the self-consistent tight-binding value of 0.8 eV. For comparison, the value of V^{ext*} obtained in a tight-binding calculation without self-consistent Hartree level screening was 70 meV.

It is of experimental interest to determine the robustness of our results to small changes in the form of V^{ext}. We consider the effect of a small bias voltage V^{bias} = 10 meV between the two graphene layers

$$V_i^{ext} = V^{ext}\sin\left(\frac{2\pi x_i}{L}\right) \pm \frac{V^{bias}}{2} \qquad (9)$$

where the $\pm$ sign refers to the two different layers. Our self-consistent tight-binding results with eqs 6 and 7 appropriately reflecting the different charges on the two layers (Figure 4) indicate that apart from the opening of a small band gap at $V^{ext} <$ 1 eV and at $V^{ext} >$ 3.9 eV, the results are very similar to the case where $V^{bias} = 0$. The opening of the small band gap is consistent with the behavior of bilayer graphene (without any lateral external periodic potential) under the influence of a transverse electric field,[18] where a gap opening occurs because of the symmetry breaking effect of the applied electric field.

The generation of new Dirac points and the opening of the band gap for $V^{ext} > V^{ext*}$ is likewise not a consequence of any special symmetries of the external periodic potential. Even though the potential $V_i^{ext} = V^{ext}\sin(2\pi x_i/L)$ has the special symmetries $V(x) = -V(-x)$ and $V(L/2 + x) = V(L/2 - x)$, we find that the breaking of either of these symmetries does not affect our results significantly. Using a potential of the form

$$V_i^{ext} = V^{ext}\sin(2\pi x_i/L) + V_i^{SB}$$
$$V_i^{SB} = \begin{cases} V^{SB} & 0 < x_i - \dfrac{L}{4} < a \\ -V^{SB} & -a < x_i - \dfrac{L}{4} < 0 \\ 0 & \text{otherwise} \end{cases} \qquad (10)$$

where a is a variable length less than $L/4$ and $V^{SB} < V^{ext}/10$ is the magnitude of the symmetry breaking potential, we obtain from tight-binding calculations that the two main features, (1) Dirac point generation for $V^{ext} < V^{ext*}$ and (2) opening of a band gap for $V^{ext} > V^{ext*}$, persist. We thus expect these to be salient features of a large class of superlattice potentials on Bernal bilayer graphene.

A modification of the perturbation theory argument following eq 4 can be used to show that deviations from uniformity of $V(x)$ along the y direction do not affect the presence of Dirac points for $V < V^*$, as long as these deviations have a length scale much larger than L. Consider a sinusoidal superlattice potential with a perturbation of the form $\Delta V(x,y) = \Delta V \sin(2\pi x/L) f(y)$. By analogy with eq 4, this results in a second order change to the energy of the conduction band of

$$E_c^{(2)}(\vec{k}) = \sum_{\substack{i=c,v \\ \vec{p}}} \frac{|\Delta V_{\vec{k}, \vec{k}+\vec{p}}^{c,i}|^2}{E_c^{(0)}(\vec{k}) - E_i^{(0)}(\vec{k} + \vec{p})} \qquad (11)$$

The sum is over all wavevectors $\vec{p}$ which are linear combinations of $\vec{G}_0 = (2\pi/L)\hat{x}$ the superlattice reciprocal lattice vector, and $p_y\hat{y}$, the various Fourier components of $f(y)$. If $f(y)$ is slowly varying compared to the superlattice potential, then the relevant wavevectors in the Fourier transform of $f(y)$ are $p_y \ll (2\pi/L)$. This implies that $\Delta V_{\vec{k},\vec{k}+\vec{p}}^{c,v} \approx 0$ and $\Delta V_{\vec{k},\vec{k}+\vec{p}}^{c,c} \neq 0$ in eq 11. $E_c^{(2)}(\vec{k})$ is therefore negative and $E_v^{(2)}(\vec{k})$ positive, as before, leading to the formation of Dirac points.

Thus far, we have considered a fixed L, and investigated the effect of varying V^{ext}. We have found that a combined variation of both L as well as V^{ext} does not introduce any new features other than those already discussed. From the point of view of the 2-band Hamiltonian (eq 1), this system is invariant under the scaling

$$\begin{aligned} L &\rightarrow \alpha L \\ V &\rightarrow \frac{V}{\alpha^2} \end{aligned} \qquad (12)$$

and can be well described by the single parameter VL^2. This is different from the case of monolayer graphene superlattices, where the analogous parameter[11−13] is VL. In the bilayer system, the effect of increasing L is to decrease the value of V^* and the value of the band gap. At the self-consistent Hartree level, this observation is still true, although the scaling behavior of eq 12 no longer holds exactly. Despite the breakdown of exact scaling behavior, we find that the general trend of decreasing bandgap and V^{ext*} with increasing L remains true.

In summary, we have shown that the application of periodic potentials to bilayer graphene can give rise to interesting physical phenomena such as the generation of new Dirac points in the low energy band structure and the opening of a band gap at a critical voltage V^{ext*}. The possibility of generating new Dirac fermions at arbitrarily low external potentials is an appealing feature of this system, given that new Dirac fermions in monolayer graphene can only be generated at strong superlattice potentials. These findings are shown to be a result of the pseudospin structure of the wave functions in bilayer graphene. The essential features of the results are robust against changes in the specific form of the external potential as well as the presence of a bias voltage between the two layers.

■ AUTHOR INFORMATION

Corresponding Author
*E-mail: sglouie@berkeley.edu.

■ REFERENCES

(1) Zhang, Y.; Tan, Y.; Stormer, H. L.; Kim, P. *Nature* **2005**, *438*, 201–204.

(2) Novoselov, K. S.; Geim, A. K.; Morozov, S. V.; Jiang, D.; Katsnelson, M. I.; Grigorieva, I. V.; Dubonos, S. V.; Firsov, A. A. *Nature* **2005**, *438*, 197–200.

(3) Gusynin, V. P.; Sharapov, S. G. *Phys. Rev. Lett.* **2005**, *95*, 146801.

(4) McCann, E.; Fal'ko, V. I. *Phys. Rev. Lett.* **2006**, *96*, 086805.

(5) Nilsson, J.; Castro Neto, A. H.; Guinea, F.; Peres, N. M. R. *Phys. Rev. B* **2008**, *78*, 045405.

(6) Pereira, V. M.; Castro Neto, A. H. *Phys. Rev. Lett.* **2009**, *103*, 046801.

(7) Ni, Z. H.; Yu, T.; Lu, Y. H.; Wang, Y. Y.; Feng, Y. P.; Shen, Z. X. *ACS Nano* **2008**, *2*, 2301–2305.

(8) Ponomarenko, L. A.; Schedin, F.; Katsnelson, M. I.; Yang, R.; Hill, E. W.; Novoselov, K. S.; Geim, A. K. *Science* **2008**, *320*, 356–358.

(9) Sols, F.; Guinea, F.; Neto, A. H. C. *Phys. Rev. Lett.* **2007**, *99*, 166803.

(10) Han, M. Y.; Ozyilmaz, B.; Zhang, Y.; Kim, P. *Phys. Rev. Lett.* **2007**, *98*, 206805.

(11) (a) Park, C.; Yang, L.; Son, Y.; Cohen, M. L.; Louie, S. G. *Nat. Phys.* **2008**, *4*, 213–217. (b) Park, C.; Son, Y.; Yang, L.; Cohen, M. L.; Louie, S. G. *Nano Lett.* **2008**, *8*, 2920–2924. (c) Park, C.; Son, Y.; Yang, L.; Cohen, M. L.; Louie, S. G. *Phys. Rev. Lett.* **2009**, *103*, 046808–4.

(12) Park, C.-H.; Tan, L. Z.; Louie, S. G. *Physica E* **2011**, *43*, 651–656.

(13) Brey, L.; Fertig, H. A. *Phys. Rev. Lett.* **2009**, *103*, 046809.

(14) Barbier, M.; Vasilopoulos, P.; Peeters, F. M.; Pereira, J. *Phys. Rev. B* **2009**, *79*, 155402.

(15) Barbier, M.; Vasilopoulos, P.; Peeters, F. M. *Phys. Rev. B* **2010**, *82*, 235408.

(16) McCann, E.; Fal'ko, V. I. *Phys. Rev. Lett.* **2006**, *96*, 086805.

(17) McCann, E. *Phys. Rev. B* **2006**, *74*, 161403.

(18) Min, H.; Sahu, B.; Banerjee, S. K.; MacDonald, A. H. *Phys. Rev. B* **2007**, *75*, 155115.

(19) Zhang, Y.; Tang, T.; Girit, C.; Hao, Z.; Martin, M. C.; Zettl, A.; Crommie, M. F.; Shen, Y. R.; Wang, F. *Nature* **2009**, *459*, 820–823.

(20) Tan, L. Z.; Park, C.; Louie, S. G. *Phys. Rev. B* **2010**, *81*, 195426.

(21) Masir, M. R.; Vasilopoulos, P.; Matulis, A.; Peeters, F. M. *Phys. Rev. B* **2008**, *77*, 235443–11.

(22) Masir, M. R.; Vasilopoulos, P.; Peeters, F. M. *Phys. Rev. B* **2009**, *79*, 035409–8.

(23) De Martino, A.; Dell'Anna, L.; Egger, R. *Phys. Rev. Lett.* **2007**, *98*, 066802–4.

(24) Dell'Anna, L.; De Martino, A. *Phys. Rev. B* **2009**, *79*, 045420–9.

(25) Kormanyos, A.; Rakyta, P.; Oroszlany, L.; Cserti, J. *Phys. Rev. B* **2008**, *78*, 045430–8.

(26) Oroszlany, L.; Rakyta, P.; Kormanyos, A.; Lambert, C. J.; Cserti, J. *Phys. Rev. B* **2008**, *77*, 081403–4.

(27) Geim, A. K.; Novoselov, K. S. *Nat. Mater.* **2007**, *6*, 183–191.

(28) Ozyilmaz, B.; Jarillo-Herrero, P.; Efetov, D.; Abanin, D. A.; Levitov, L. S.; Kim, P. *Phys. Rev. Lett.* **2007**, *99*, 166804–4.

(29) Marchini, S.; Gunther, S.; Wintterlin, J. *Phys. Rev. B* **2007**, *76*, 075429.

(30) Sutter, P. W.; Flege, J.; Sutter, E. A. *Nat. Mater.* **2008**, *7*, 406–411.

(31) Coraux, J.; ǸDiaye, A. T.; Busse, C.; Michely, T. *Nano Lett.* **2008**, *8*, 565–570.

(32) N'Diaye, A. T.; Coraux, J.; Plasa, T. N.; Busse, C.; Michely, T. *New J. Phys.* **2008**, *10*, 043033.

(33) Pletikosić, I.; Kralj, M.; Pervan, P.; Brako, R.; Coraux, J.; N'Diaye, A. T.; Busse, C.; Michely, T. *Phys. Rev. Lett.* **2009**, *102*, 056808.

(34) Meyer, J. C.; Girit, C. O.; Crommie, M. F.; Zettl, A. *Appl. Phys. Lett.* **2008**, *92*, 123110–3.

(35) Mañes, J. L.; Guinea, F.; Vozmediano, M. A. H. *Phys. Rev. B* **2007**, *75*, 155424.

(36) Latil, S.; Meunier, V.; Henrard, L. *Phys. Rev. B* **2007**, *76*, 201402.

(37) Lopes dos Santos, J. M. B.; Peres, N. M. R.; Castro Neto, A. H. *Phys. Rev. Lett.* **2007**, *99*, 256802.

(38) Hass, J.; Varchon, F.; Millán-Otoya, J. E.; Sprinkle, M.; Sharma, N.; de Heer, W. A.; Berger, C.; First, P. N.; Magaud, L.; Conrad, E. H. *Phys. Rev. Lett.* **2008**, *100*, 125504.

(39) Mele, E. J. *Phys. Rev. B* **2010**, *81*, 161405.

(40) (a) Bistritzer, R.; MacDonald, A. H. *Phys. Rev. B* **2010**, *81*, 245412. (b) Bistritzer, R.; MacDonald, A. H. arxiv:1009.4203, 2010.

(41) de Gail, R.; Goerbig, M. O.; Guinea, F.; Montambaux, G.; Neto, A. H. C. arxiv:1103.3172, 2011.

(42) Killi, M.; Wu, S.; , Paramekanti, A. arxiv: *1104.0051,* 2011.

■ NOTE ADDED IN PROOF

After submission of our manuscript, we became aware of a related work that contains results consistent with ours.[42]